Received: 9 July 2018 | Revised: 18 September 2018 | Accepted: 12 November 2018

DOI: 10.1002/sia.6597

RESEARCH ARTICLE

WILEY SURFACE and INTERFACE ANALYSIS

Experimental investigation of the adhesion force of single and double-layer coatings on MEMS surfaces

Mahdi Joulaei[1] | Mojtaba Kolahdoozan[1] | Mehdi Salehi[1] | Mehdi Zadsar[2] | Meisam Vahabi[1]

[1] Department of Mechanical Engineering, Najafabad Branch, Islamic Azad University, Najafabad, Iran

[2] Department of Physics, Najafabad Branch, Islamic Azad University, Najafabad, Iran

Correspondence
Mojtaba Kolahdoozan, Department of Mechanical Engineering, Modern Manufacturing Technologies Research Center, Najafabad Branch, Islamic Azad University, Najafabad, Iran.
Email: kolahdoozan@pmc.iaun.ac.ir

Adhesion force is one of the most important factors in microelectromechanical systems (MEMS), especially for microassembly. It depends on operating conditions and is affected by the contact area. In this study, the adhesion force between MEMS materials and AFM tips was analysed using AFM's point-mode spectroscopy. The aim was to study the effectiveness of various coatings in MEMS adhesion surfaces. For this purpose, five silicon surfaces were used, four of which were coated, and one was noncoated. Two of them were deposited by single-layer coating (Au and Ag). The other two were deposited by double-layer coating (TiO_2/Au, TiO_2/Ag) on a Si (1 0 0) substrate. The depositing was accomplished by the thermal evaporation method. Composite materials and analysis were reviewed by observing the SEM image. The experimental results showed that the method of deposition helped to decrease the adhesion force between the probe tip and the surface of the specimens, and double-layer coating had stronger effect on decreasing the adhesion force than the single-layer coating.

1 | INTRODUCTION

In recent years, the increasing use of microelectromechanical system (MEMS) devices and new fields like microassembly has resulted in decrease of adhesion force in the devices employed for capturing, safe holding, transferring, and releasing microparts such as microgrippers.[1-5] The effective force on the adhesion of surface in the MEMS are Van der Waals force as well as capillary and electrostatic force, prevailing the weight of the parts.[4-8]

One way to reduce the adhesion force is to reduce the effective surface between two involved surfaces. While some studies have shown that decreasing the interfacial roughness can increase adhesion, coating can also be useful.[9] In most of the studies, silicon is used as one of the most suitable materials in MEMS for the chosen surface.[2,5,10]

Other researches have studied the effect of surface roughness and the particles size on the adhesion.[8,11-14] In addition, the effect of decreasing the pull-off force on the roughness of surface of microgrippers has been investigated by the fabrication of the polymeric coating deposited.[1,2]

According to the studies conducted on the deposition of polymeric films, the method of Deeping[1,2] is implemented; for the nonpolymeric films, a method like atomic layer deposition (ALD)[12] is applied. The high potential and velocity of the coating, the precise control of the thickness of the film, and the high quality of this thin layer are the advantages of the ALD coating. However, as a major disadvantage of this method, it requires a plasma environment.[12] The specimens' deposition was performed by using the thermal evaporation method on the surface. It is a gas method of phase deposition with many uses in the MEMS/NEMS, particularly for microfabrication.[15-20] With this method, the thin layer of coating is monotonous and shows the best adhesion on the substrate and high quality, without the need for the plasma environment.[15-20]

The most important property of the MEMS appliances is their high electricity transmission. Therefore, coating materials should have high conductivity and low surface adhesion. Accordingly, many studies have addressed coatings of gold and silver on the silicon substrate.[21,22]

Titanium dioxide grows in a crystalline manner, and has a high dielectric constant, acting as the protective layer in diverse chemical

environments.[23] TiO_2 films have properties such as better durability, high refractive index, and high optical transmittance, making them suitable for multilayer thin film device applications.[24] TiO_2 thin films improve the surface smoothness, surface morphology, crystallization phases, and growth rates, maintaining the high functional quality. TiO_2 thin films suitable for applications of MEMS containing stress are micromachined by dry etching and wettability conversion. These investigations indicate that smooth TiO_2-based MEMS devices with mechanical properties can be realized.[25-27]

However, improving the reliability, titanium dioxide coating is obtained at the expense of reduction in the surface adhesion force and energy.[28] Double-layer coatings cause a change in the roughness of the substrate, affecting the properties of the surface layer.[29]

In the experimental studies, an atomic force microscope (AFM) and a force-level device (SFA) have been used to obtain the adhesion force. The force measurement with the AFM, due to its high resolution, allows observation and manipulation of molecular and atomic surface features.[22]

The AFM is armed with a cantilever with a sharp tip at its free-swinging end. This tip is driven toward the surface of the investigated specimen, and due to the interaction occurring between the tip and the specimen, the cantilever is bent. Using a detector and a laser, the bending and/or orbital deviation of the cantilever can be determined.[30]

The surface topographic features provided by AFM include surface topography and the main statistical surface parameters.[31] The AFM can be used to distinguish dependence of the interaction on the probe-specimen distance at a certain place. The spectroscopy can be displayed as a local force spectroscopy (to measure the mechanical properties of the specimen) or as a force imaging spectroscopy. In the first case, a plot of the deflection of the cantilever against the specimen displacement is obtained for a special point on the specimen surface. The force can be easily calculated by knowing the spring constant of the cantilever. In the second case, the plots are generated for a large number of points on the specimen surface. This kind of spectroscopy can be applied to measure adhesion, hardness, or deformability of specimens and Van der Waals interactions.[32]

Scanning electron microscope (SEM) image of a composite material includes visible morphological structures with similar clusters of its constituent particles immiscible with the material basis. SEM images display the structures characterized in terms of their forms, sizes, material, and uniformity of the layer.[33-36]

In this article, gold and silver were coated on the silicon surfaces using the thermal evaporation method, by single-layer and double-layer depositing; the first layer material on the double-layer coatings was TiO_2; AFM measurements considered for this article were measurements related to the minimum force necessary to separate the AFM tip. The specimen giving the adhesion force is often known as the pull-off force. Experimental researches of this article were performed using the spectroscopy in the AFM point mode. The purpose was to determine the adhesion force between the AFM tip and the surfaces of the specimens; then, the adhesion force of the obtained specimens was compared, and the effect of the double-layer coatings on reduction of the surface adhesion force was demonstrated. In this work, SEM image for analysis of the structures of depositions included size and percent of materials on the surface.

2 | MATERIALS AND EXPERIMENTAL PROCEDURE

2.1 | Surface and materials

The materials investigated in this work were thin solid films of gold, silver, and titanium dioxide with the thickness of 150 and 100 nm. This thickness of coating usually was used in MEMS especially in microassemblies and the process of making microgrippers.[2,12,21,37]

The substrate for all specimens was single crystal (monocrystal) silicon <100>. For this purpose, five silicon wafers polished were given in the size of 8 × 8 × 0.5 mm.

One of the silicon specimens was not coated to compare it with other coated ones. Figure 1A is the schematic picture of a noncoated specimen. Two specimens of silicon wafers were given the single-layer coating, and two other silicon wafers received the double-layer

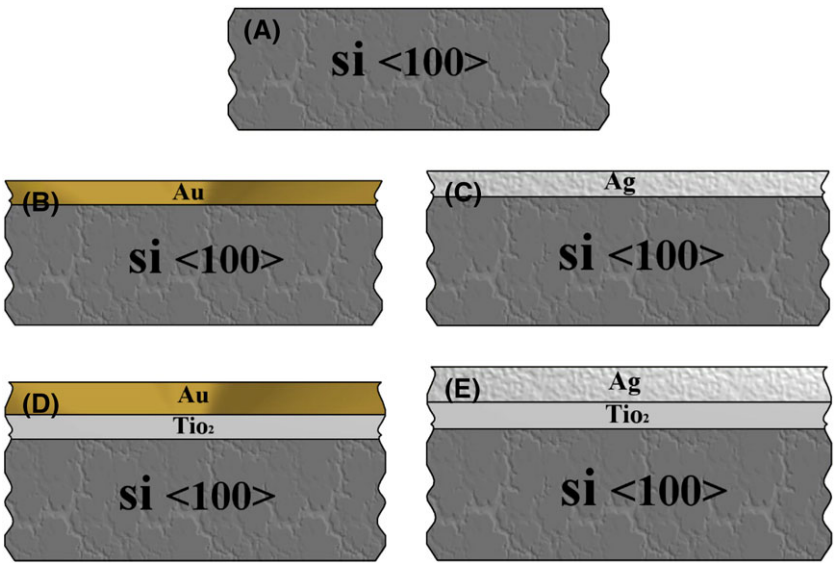

FIGURE 1 A, Schematic picture of a noncoated specimen. B, Schematic picture of the specimen of the single-layer coated by gold. C, Schematic picture of the specimen of the single layer coated by silver. D, Schematic picture of the specimen of double layer coated by titanium dioxide and gold. E, Schematic picture of the specimen of the double layer coated by titanium dioxide and silver

coating. As Figure 1B shows, single-layer coatings were made of gold, and the second layer was coated by silver. The schematic picture of the single-layer made by gold coating is provided. Figure 1C presents the schematic picture of the single-layer silver coating. As Figure 1D depicts, double-layer coatings were the primary layer with titanium dioxide coating, and the next layer was the one with gold and silver coating. The schematic picture of the double-layer coating by the titanium dioxide and gold is provided. Figure 1E displays the schematic picture of the double-layer coating by the titanium dioxide and silver. Additionally, Table 1 shows the materials and thickness of each of the specimens.

2.2 | Details of deposition

The thermal evaporation coating is a process in a vacuum environment by which the source material evaporates by applying an electric current and transfers to the substrate by the pressure difference between the source material and the substrate. Controllable parameters in this process are the pressure of the chamber and the temperature of the filament boat. This method of deposition is one of the most common types of coating in thin film layers.[15-20]

The thickness of the layers and evaporation rate were measured using quartz crystal microbalance. The system includes a silicate and a crystalline holder. The measurement accuracy is 1 nm that can measure and control the thickness of the layer in during of coating process.[38]

Before deposition, the silicon substrate was washed with boiling water, deionized water, ethanol, acetone, propanol, and isopropyl alcohol. Then, they were dried with nitrogen. The thin film deposition was carried out by the thermal evaporation method. With the thickness monitor of quartz crystals, the layer thickness and the layer deposition rate were controlled. Table 2 displays the details of the coating of each of the depositions.

2.3 | SEM imaging

SEM imaging was carried out by scanning on all of the specimens with a focused beam of electrons. The electrons produced several signals that could be detected; they included information about surface topography and combination of the specimens. The SEM images only confirm the presence of coated layer. The electron beam is usually scanned in a raster scan pattern, and the beam's position is combined with the detected signal to produce an image.

SEM images of all specimens were taken by the FE-SEM microscope. The optimum contrast of the images was found for an accelerating voltage of 15 kV at a nominal working distance of 10 mm. Table 3 shows the analysis conditions.

Figure 2A shows the dispersion of gold particles on the silicon substrate in the SEM image. In this image, the colour of gold particles was white, and the silicon substrate (background) was grey. Figure 2B shows the dispersion of silver particles on the silicon substrate in the SEM image. In this image, the colour of silver particles was white, and the silicon substrate (background) was grey. Figure 2 C shows the dispersion of titanium dioxide and gold particles on the silicon substrate in the SEM image. In this image, the colour of the titanium dioxide and gold particles was white, and the silicon substrate (background) was grey. Figure 2D shows the dispersion of titanium dioxide and silver particles on the silicon substrate in the SEM image. In this image, the colour of the titanium dioxide and silver particles was white, and the silicon substrate (background) was grey.

2.4 | Experimental procedure

The details of the thin films at nanoscale were applied using an AFM NanoWizard II (JPK Instruments, Germany) in the atomic force

TABLE 1 Materials and thickness of all investigated specimens

Specimen Number	Substrate	First Layer	Thickness	Second Layer	Thickness
1	Si (100)	-	-	-	-
2	Si (100)	Au	100 nm	-	-
3	Si (100)	Ag	100 nm	-	-
4	Si (100)	TiO_2	150 nm	Au	100 nm
5	Si (100)	TiO_2	150 nm	Ag	100 nm

TABLE 2 Characteristics of each layer

No.	Layer	Thickness	Purity	Temperature	Pressure
1	Au	100 nm	99.99%	40°C	6×10^{-6} mbar
2	Ag	100 nm	99.99%	40°C	6×10^{-6} mbar
3	TiO_2	150 nm	99.9%	40°C	6×10^{-6} mbar

TABLE 3 Analysis conditions

Accelerating Voltage, kV	Beam Current, nA	Magnification	Live Time, s	Preset Time, s	Nb Channels	Ev/Channel	Offset, keV	Width, keV
15.0	10.000	100 000	16	30	1024	20	0	20

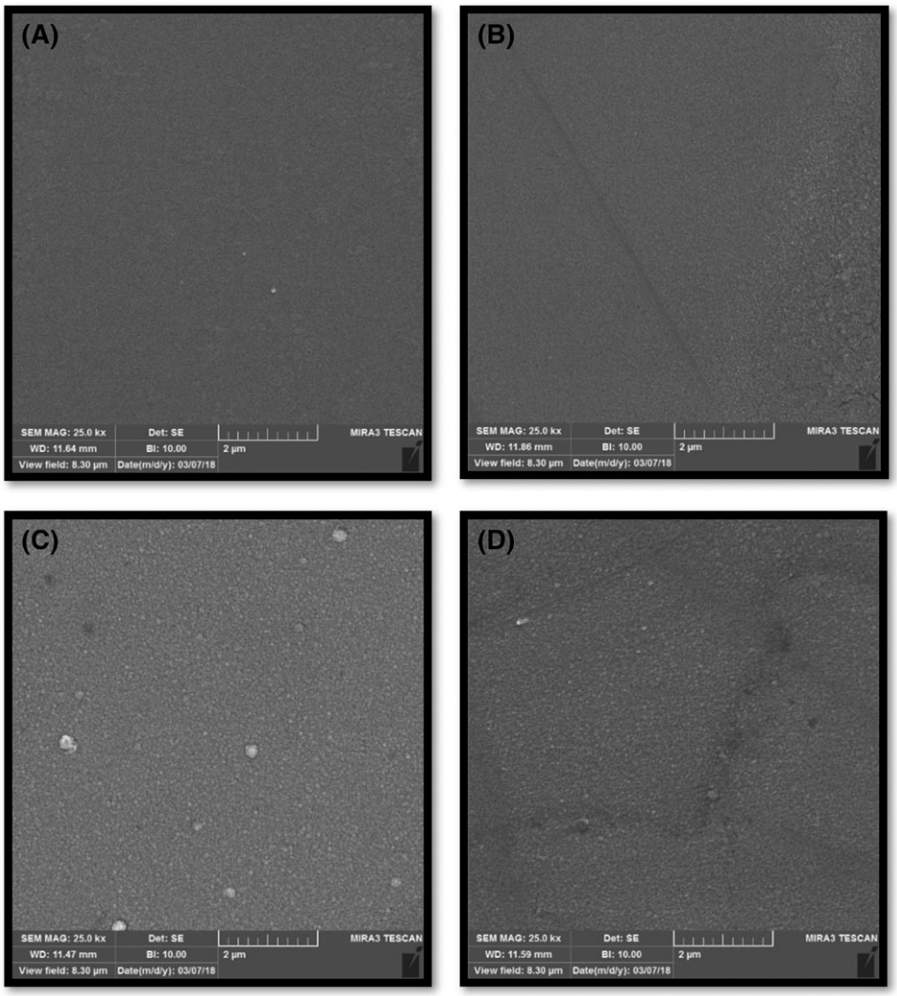

FIGURE 2 A, SEM image of the Au thin film (specimen 2). B, SEM image of the Ag thin film (specimen 3). C, SEM image of the TiO_2/Au thin film (specimen 4). D, SEM image of the TiO_2/Ag thin film (specimen 5)

microscope laboratory. The investigations were conducted at a temperature of 23°C and a scanning frequency of 0.74 Hz. The probe model used for these tests was a HYDRA V-Shaped Probe Series (Hydra 6V-100NG), which according to the manufacturer's specifications, it had the length of 100 µm, the width of 18 µm, the thickness of 0.6 µm, the spring constant of 0.292 N/m, and the resonance frequency of 66 kHz. The cantilever had specifications of a material with low stress silicon nitride and a V shape. The tip had the specifications of a material of Si, a tetrahedral shape, the height of 4 to 6 µm, and the ROC of <10 nm.

In the AFM technique, a sharp tip attached to the cantilever scans the specimen surface. The force between the tip and the specimen surface bends the cantilever during the scanning. A detector measures the size of this deviation. Based on this deviation, forces between the tip and the surface (experimental force or pull of force) are estimated.[30]

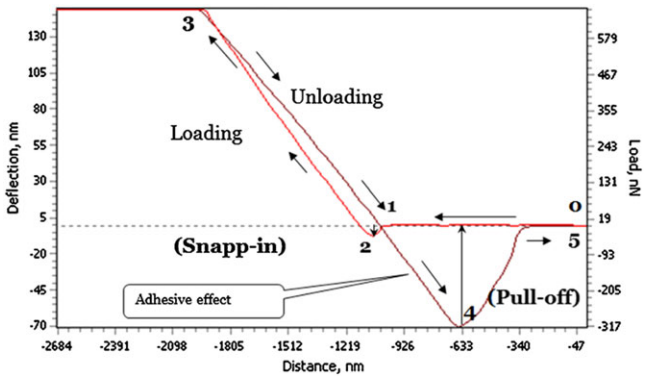

FIGURE 3 The AFM curve of loading and unloading using spectroscopy in the point mode[37]

AFM curves obtained are presented in Figure 3. With the reduction of the distance between the tip of AFM and the specimen surface (by applying the force from the piezoelectric to the cantilever), the tip of AFM and the specimen surface will be contacted at one point such that neither of them can move. By applying pressure from the tip to the specimen, the force increases linearly until a distance of the tip from the specimen reaches a certain limit. After this point, the amount of the applied force decreases from the specimen to the AFM tip. The calculated force is converted from pressure to the traction (repulse). At this moment, due to the repulsive force between the tip and the specimen, the tip of the probe is separated from the specimen and, at a balance distance, the force between the tip and the specimen

becomes zero. From this moment on, the tip takes distance from the surface specimen, and the applied force between them becomes gravitational. The amount of this force is shown in Figure 3.[30,37]

In Figure 3, from point 0 to 1, the tip and the specimen surface were without contact; from point 1 to 2, the tip was under the influence of gravity or traction forces; in point 3, under the loading of an atomic force microscope, the tip drops down inside the surface or the tip be deformed; in point 4, due to the removal effect of the load, an adhesion effect is created between the tip and the specimen. This leads to the impact (to the extent of failing) to the tip from the surface; finally, in point 5, the tip returns to its initial place.[30,37] Figure 3 presents experimental adhesion force measured for 49 points for each specimen obtained.

The experimental curves rendering the dependence between the force used and the movement of the piezo table were obtained for all the specimens. Based on these curves, the values of the minimum, maximum, mean, and total of the adhesion force between the AFM tip and each specimen were obtained.

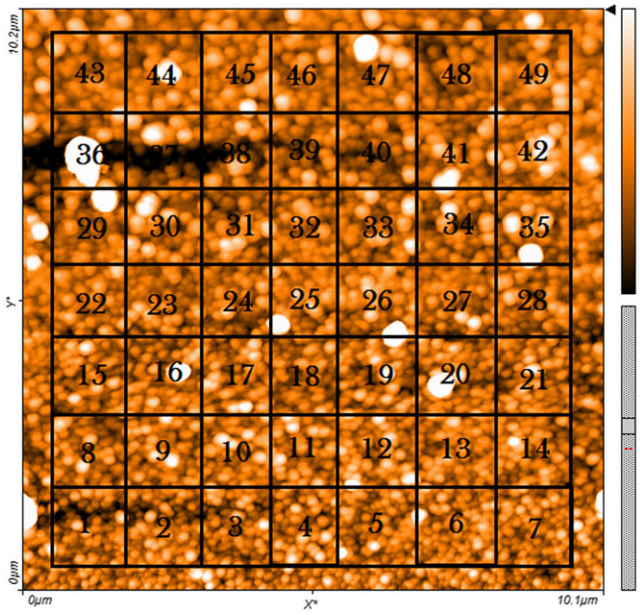

FIGURE 4 The image of a specimen obtained with the XEI image processing tool for SPM data

3 | RESULTS AND DISCUSSION

According to the SEM images (Figure 2A to 2D), for each specimen, the uniformity of the layers and particle sizes could be clearly observed on the nanometer/micrometer length scale. Table 4 specifies the percent mass and area of the materials on the specimen surface in SEM images. *W*% represents the percent of the mass, and *A*% shows the percent of the area in the tested portion.

For each specimen, a grid of 49 squares was considered (Figure 4), and the adhesion force was specified from the minimum value of the experimental curves obtained by the JPK SPM software for the centre of each square.

Figure 5 presents the results of the experimental adhesion force of all centres of each square (in Figure 4) over the surface of specimens. As Figure 5A shows, in the silicon <100> noncoated, the experimental adhesion force was obtained to be between 9 and 28 nN. As Figure 5B shows, in the Au thin film, the experimental adhesion force was between 16.5 and 25.8 nN. In the Ag thin film, as Figure 5C shows, the experimental adhesion force was between 7.4 and 38.2 nN. In the case of TiO_2/Au thin film, as Figure 5D shows, the experimental adhesion force was between 4 and 38.8 nN. As Figure 5E depicts, regarding the TiO_2/Ag thin film, the experimental adhesion force was between 2.5 and 39.5 nN.

TABLE 4 Percent of mass and area of the materials in SEM images

Specimen Number	Coating Material	*W*%	*A*%
1	Au	100% Au	100% Au
2	Ag	100% Ag	100% Ag
3	TiO_2/Au	38.71% O 8.98% Ti 52.31% Au	71.26% O 4.66% Ti 24.08% Au
4	TiO_2/Ag	25.11% O 7.12% Ti 67.77% Ag	61.22% O 2.43% Ti 36.35% Ag

For each specimen, Table 5 shows the minimum, maximum, and mean values of the experimental adhesion force and the total experimental force.

The results of the values obtained in Figures 5 and Table 5 indicated that single-layer coatings had less force values, as compared with the uncoated specimens, and the effect of double-layer coatings was more evident in reduction of the adhesion force. In Table 5, the last two columns correspond to the variance and standard deviation. In uncoated and gold specimens, the data scattering is lower than other specimens and double-layer coatings have the highest scattering. These scatterings can have a direct relationship with surface roughness variables. Figure 6 shows comparison of the mean value of the adhesion forces of the specimen's surfaces.

The main parameters influencing adhesion force are the surface energy, the surface roughness, and the radius, shape, and material of the AFM tip. In this article, shape and material of the AFM tip were constant, and two other parameters were changed.

Roughness is a property of the material surface texture where its roughness topography is identified with an ideal flat surface. A rough surface contains protuberance and depressions at near distance from each other. The greater this roughness is, the greater the protuberance, depressions, the height of the waves, and the waves of the sharp tip in the surface. As a result, the actual contact and the adhesion force between the two surfaces reduce. There are many studies on reducing adhesion force by an increase in surface roughness parameters.[12,21,37]

The surface energy is defined as the sum of all intermolecular forces that are on the surface of a material. In other words, it is the degree of attraction or repulsion force a material surface exerts on another material. This energy has a direct relationship with the surface adhesion force.[37]

In experimental investigation (in Figure 6), single-layer coatings of gold and silver compared with silicon of noncoated had less adhesive force due to the effect of surface energy and surface roughness on

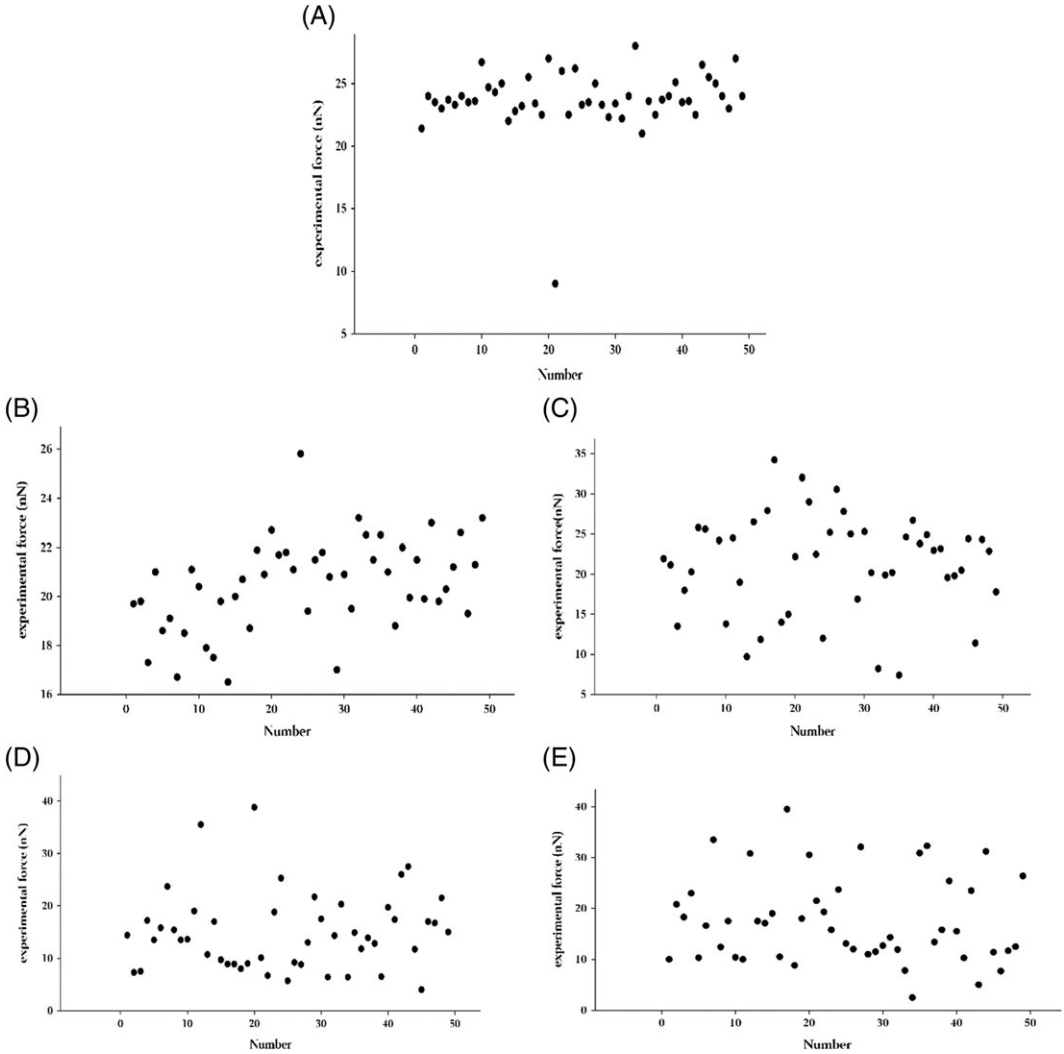

FIGURE 5 A, The experimental forces of the silicon <100> noncoated (specimen 1). B, The experimental forces of the Au thin film (specimen 2). C, The experimental forces of the Ag thin film (specimen 3). D, The experimental forces of the TiO_2/Au thin film (specimen 4). E, The experimental forces of the TiO_2/Ag thin film (specimen 5)

TABLE 5 Min, max, total, and mean values of adhesion force of the specimens along with variance and standard deviation

Specimens	Minimum Adhesion Force, nN	Maximum Adhesion Force, nN	Total of Adhesion Forces, nN	Mean Values of Adhesion Force, nN	Variance	Discussion of Standard Deviation
1. Noncoating	9	28	1160.3	23.6	6.7	2.6
2. Au	16.5	25.8	1003.65	20.5	3.5	1.9
3. Ag	7.4	38.2	1056.46	21.56	42	6.5
4. TiO_2/Au	4	38.8	728	14.86	53	7.3
5. TiO_2/Ag	2.5	39.5	856.7	17.48	70.8	8.4

the adhesion force. The surface energy of silicon, silver, and gold was 2130,[39] 1130,[40] and 1400[40] MJ/m^2, respectively, and the average surface roughness (Ra) of silicon, silver, and gold was 0.8, 1.65, and 1.9 nm, respectively. To obtain the surface roughness results, atomic force microscopy (AFM) was applied. By comparing the surface energy of specimens of single-layer coating (silver thin film and gold thin film) and noncoated, the maximum surface energy is related to silicon of noncoated; therefore, single-layer coatings reduced the surface energy of the specimen. By comparing the roughness of the surface of the three specimens, single-layer coatings of the surface parameter of roughness average, Ra, increased. Therefore, two parameters of surface energy and surface roughness were the reason for reduction of the surface adhesion force at single-layer coating than the noncoated specimen.

In experimental investigation (in Figure 6), double-layer coatings of TiO_2/Au and TiO_2/Ag compared with single-layer coatings had less surface adhesive force. The double-layer coating of TiO_2/Au and the single-layer coating of Au, due to equality of the last layer (upper

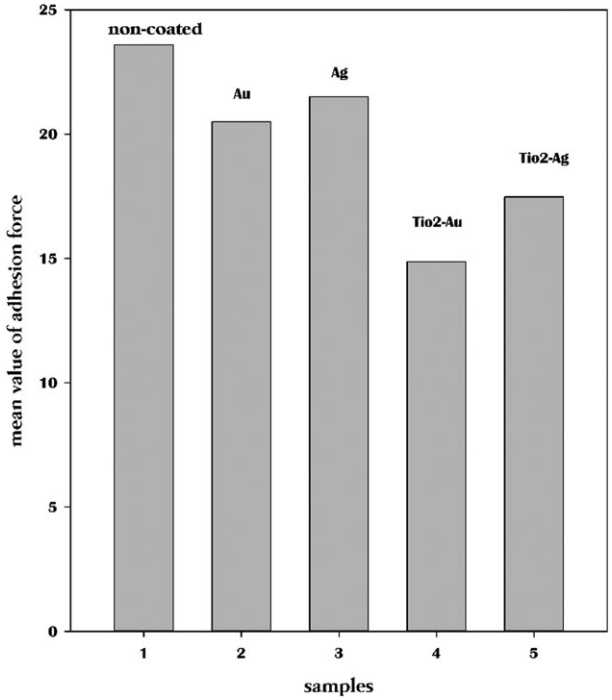

FIGURE 6 Mean values of adhesion force for each specimen

TABLE 6 The reasons for reducing the surface adhesion force for each specimen

Specimens	Compared with	The Reasons for the Reduction of the Surface Adhesion Force
Noncoating	-	-
Au	Noncoating	The increase in roughness + reduction of the surface energy
Ag	Noncoating	The increase in roughness + reduction of the surface energy
TiO_2/Au	Au	The increase in roughness
TiO_2/Ag	Ag	The increase in roughness

layer), have the same surface energy, but the roughness of the TiO_2/Au coating is due to the presence of titanium dioxide between the silicon substrate and the upper layer, causing increase of average surface roughness (Ra = 6.5 nm), and consequently reduction of the surface adhesion force. Similarly, TiO_2/Ag coating and Ag coating have the same surface energy, but average surface roughness (Ra) of TiO_2/Ag coating is due to the presence of titanium dioxide between the silicon substrate and the upper layer, causing increase of average surface roughness (Ra = 5.6 nm), and consequently reduction of the surface adhesion force. Single-layer and double-layer coatings of gold, compared with silver, have the least surface adhesive force due to their higher surface roughness (Ra).

4 | CONCLUSIONS

Reduction of the surface adhesion on the microelectromechanical systems is important, especially in microassembly. In this article, the effects of different layers of surface deposition on the adhesion force between atomic force microscopy probe and surfaces were investigated.

In all experiments, microscope probes, environmental conditions, substrate, and method of deposition (thermal evaporation) were constant, and material of layer was changed. The aim of the deposition was to reduce the surface adhesion force by changing surface energy and parameters of surface roughness.

Deposition of layer was carried out in two methods. Single-layer coatings were the first method, which their effect on reduction of surface adhesion force has been proven in this paper and previous researches.[1,2,21,22,37,41] The second method is a double-layer deposition that is a new method to reduce the surface adhesion force, and the purpose of this method is to change the surface roughness and decrease of adhesion force; this is effective on increasing the efficiency of microassemblies and other equipments of MEMS.

The thickness of the gold and silver layer (the last layer or upper layer) in all specimens was fixed, and in the double-layer coating, the middle layer material was titanium dioxide that caused changes in the substrate surface roughness. The results indicate that the double-layer coating has been more effective in reducing adhesion force. The images of the scanning electron microscope, uniformity of depositions, and percentage of different materials of the layers were also presented.

For each specimen, Table 6 shows the reasons for reducing the surface adhesion force.

In Table 6, specimens of single-layer coating with the noncoating specimen and double-layer coating specimens are compared with specimens of the single-layer coating. The table also specifies the main reasons for the reduction of surface adhesion. Increasing surface roughness caused a reduction of the actual contact between surfaces and thus a decrease in the surface adhesion force.[12,21,37] The surface energy consists of intermolecular forces that are on the surface of a material. This energy has a direct relationship with the surface adhesion force such that a decrease in the surface energy leads to a reduction in the surface adhesion force.[37]

ACKNOWLEDGEMENTS

The authors would like to thank Mrs. Maghfourian for the AFM tests. They also appreciate Dr. Ghasemi for the deposition.

ORCID

Mojtaba Kolahdoozan https://orcid.org/0000-0001-9059-1067

REFERENCES

1. Balabanava N, Wierzbicki R, Heerlein H, Zielecka M, Rymuza Z. Low surface energy films for microgripping applications. *Microelectron Eng*. 2006;83(4–9):1389-1392.
2. Balabanava N, Wierzbicki R, Zielecka M, Rymuza Z. Effect of roughness on adhesion of polymeric coatings used for microgrippers. *Microelectron Eng*. 2007;84(5–8):1227-1230.
3. Agnus J, Hériban D, Gauthier M, Pétrini V. Silicon end-effectors for microgripping tasks. *Precis Eng*. 2009;33(4):542-548.
4. Sanchez AJ. Handling for micro-manufacturing. In: Qin Y, ed. *Micromanufacturing engineering and technology*. Kidlington: Elsevier; 2010:298-314.

5. Sausse LM, Delchambre A, Re'gnier S, Lambert P. Electrostatic forces in micromanipulations: review of analytical models and simulations including roughness. *Appl Surf Sci*. 2007;253(14):6203-6210.
6. Kim SH, Asay DB, Dugger MT. Nanotribology and MEMS. *NanoToday*. 2007;2(5):22-29.
7. Bhushan B. Nanotribology and nanomechanics. *Wear*. 2005;259(7–12):1507-1531.
8. Serro AP, Colaco R, Saramago B. Adhesion forces in liquid media: effect of surface topography and wettability. *J Colloid Interface Sci*. 2008;325(2):573-579.
9. Salimi A. Characterization of nano scale adhesion at solid surface of oxidized PP wax/PP blends. *Int J Adhes Adhes*. 2012;33:61-66.
10. Colak A, Wormeester H, Zandvliet HJW, Poelsema B. Surface adhesion and its dependence on surface roughness and humidity measured with aflat tip. *Appl Surf Sci*. 2012;258(18):6938-6942.
11. Kudryavtsev YV, Gelinck E, Fischer HR. Theoretical investigation of van der Waals forces between solid surfaces at nanoscales. *Surf Sci*. 2009;603(16):2580-2587.
12. Katainen J, Paajanen M, Ahtola E, Pore V, Lahtinen J. Adhesion as an interplay between particle size and surface roughness. *J Colloid Interface Sci*. 2006;304(2):524-529.
13. Meine K, Kloß K, Schneider T, Spaltmann D. The influence of surface roughness on the adhesion force. *Surf Interface Anal*. 2004;36(8):694-697.
14. Lina S, Xiaoli W, Guoxin X, Na S. Nano-adhesion and friction of multi-asperity contact: a molecular dynamics simulation study. *Surf Interface Anal*. 2015;47:919-925.
15. Jazirehpour M, Bahahrvandi HR, Alizadeh A, Ehsani N. Facile synthesis of boron carbide elongated nanostructures via a simple in situ thermal evaporation process. *Ceram Int*. 2011;37(3):1055-1061.
16. Ohzono T, Monobe H. Microwrinkles: shape-tunability and applications. *J Colloid Interface Sci*. 2012;368(1):1-8.
17. Lee KC, Lee SS. Deep X-ray mask with integrated actuator for 3D microfabrication. *Sensors Actuators A: Phys*. 2003;108(1–3):121-127.
18. Lee KC, Lee SS. Deep X-ray mask with integrated electro-thermal microxystage for 3D fabrication. *Sensors Actuators A: Phys*. 2004;111(1):37-43.
19. Fang W, Lo CY. On the thermal expansion coefficients of thin films. *Sensors Actuators A: Phys*. 2000;84(3):310-314.
20. Wilson SA, Jourdain RPJ, Zhang Q, et al. New materials for micro-scale sensors and actuators: an engineering review. *Mater Sci Eng R Rep*. 2007;56(1–6):1-129.
21. Kolahdoozan M, Hamedi M, Nikkhah-Bahrami M. A novel model for the effect of geometric properties of micro/nanoscale asperities on surface adhesion. *Int J Adhes Adhes*. 2014;48:280-287.
22. Casa M, Sarno M, Liguori R, et al. Conductive adhesive based on mussel-inspired graphene decoration with silver nanoparticles. *J Nanosci Nanotechnol*. 2018;18(2):1176-1185.
23. Puurunen RL, Saarilahti J, Kattelus H. Implementing ALD layers in MEMS processing. *ECS Trans*. 2007;11(7):3-14.
24. Narasimha RK. Influence of deposition parameters on optical properties of TiO2 films. *Optical Eng*. 2002;41(9):2357-2364.
25. Huang Y, Pandraud G, Sarro PM. Characterization of low temperature deposited atomic layer deposition TiO2 for MEMS applications. *J Vac Sci Technol A*. 2013;31(1):1-8.
26. Tailor S, Rakoch AG, Gladkova AA, et al. Kinetic features of Wear-resistant coating growth on Ti-alloy by plasma electrolytic oxidation. *Surf Innov*. 2018;6(3):141-149.
27. Wang BN, Olmeijer D, Shah R, Krogman KC. Highly durable spray layer-by-layer assembled films. *Surf Innov*. 2013;1(2):92-97.
28. Lee D, Pott V, Kam H, Nathanael R, Liu TJK. AFM characterization of adhesion force in micro-relays. Micro Electro Mechanical Systems (MEMS), IEEE 23rd International Conference on 2010: 232–235.
29. Sander H, Petersohn D. Friction and wear behaviour of PVD-coated tribosystems. *Tribology Series* (Thin Films in Tribology; Edited by D. Dowson et al.). Elsevier Science Publishers BV. 1993;25:3-12.
30. Birleanu C, Pustan M, Dudescu C, Belcin O, Rymuza Z. Nanotribological investigations on adhesion effect applied to MEMS materials. *Acta Technica Napoc Ser: Appl Math, Mech Eng*. 2012;55(3):671-676.
31. Wu L, Noels L, Rochus V, Pustan M, Golinval JC. A micro-macro approach to predict stiction due to surface contact in microelectromechanical systems. *J Microelectromech Syst*. 2011;20(4):976-990.
32. Shi X, Zhao YP. Comparison of various adhesion contact theories and the influence of dimensionless load parameter. *J Adhes Sci Technol*. 2004;18(1):55-68.
33. Chitra L, Ramakrishnan V. Comparative analysis of structures and materials for the design of cantilever type MEMS humidity sensor. *J Adv Res Dyn Control Syst*. 2017;9(3):84-91.
34. Bhachu DS, Scanlon DO, Saban EJ, et al. Scalable route to $CH_3NH_3PbI_3$perovskite thinfilms by aerosol assisted chemical vapour deposition. *J Mater Chem A*. 2015;3(17):9071-9073.
35. Ibraheam AS, Al-Douri Y, Hashim U, Ameri M, Bouhemadou A, Khenata R. Structural, optical and electrical investigations of $Cu_2Zn_{1-x}Cd_xSnS_4$/Si quinternary alloy nanostructures synthesized by spin coating technique. *Microsyst Technol*. 2017;23(6):2223-2232.
36. Thomas D, Sadasivuni KK, Waseem S, Kumar B, Cabibihan JJ. Synthesis, green emission and photosensitivity of Al-doped ZnO film. *Microsyst Technol*. 2018;24(7):3069-3073.
37. Rusu F, Pustan M, Bîrleanu C, Müllerb R, Voicu R, Baracu A. Analysis of the surface effects on adhesion in MEMS structures. *Appl Surf Sci*. 2015;358:634-640.
38. Slang S, Janicek P, Palka K, Loghina L, Vlcek M. Optical properties and surface structuring of Ge20Sb5S75 amorphous chalcogenide thin films deposited by spin-coating and vacuum thermal evaporation. *Mater Chem Phys*. 2018;203:310-318.
39. Jaccodine RJ. Surface energy of germanium and silicon. *J Electrochem Soc*. 1963;110(6):524-527.
40. Zhang JM, Ma F, Xu KW. Calculation of the surface energy of FCC metals with modified embedded-atom method. *Appl Surf Sci*. 2004;229(1-4):34-42.
41. Jänchen G, Mertig M, Pompe W. Adhesion energy of thin collagen coatings and titanium. *Surf Interface Anal*. 1999;27(5-6):444-449.

How to cite this article: Joulaei M, Kolahdoozan M, Salehi M, Zadsar M, Vahabi M. Experimental investigation of the adhesion force of single and double-layer coatings on MEMS surfaces. *Surf Interface Anal*. 2019;51:419–426. https://doi.org/10.1002/sia.6597